Advances in Concrete Construction, *Vol. 16, No. 4 (2023) 205-216*
https://doi.org/10.12989/acc.2023.16.4.205

Evaluation of Near Surface Mounted (NSM) FRP technique for strengthening of reinforced concrete slabs

Chunwei Zhang* and M. Abedini [a]

Multidisciplinary Center for Infrastructure Engineering, Shenyang University of Technology, Shenyang 110870, China

(*Received November 18, 2022, Revised November 13, 2023, Accepted March 8, 2024*)

Abstract. Concrete structures may become vulnerable during their lifetime due to several reasons such as degradation of their material properties; design or construction errors; and environmental damage due to earthquake. These structures should be repaired or strengthened to ensure proper performance for the current service load demands. Several methods have been investigated and applied for the strengthening of reinforced concrete (RC) structures using various materials. Fiber reinforced polymer (FRP) reinforcement is one of the most recent type of material for the strengthening purpose of RC structures. The main objective of the present research is to identify the behavior of reinforced concrete slabs strengthened with FRP bars by using near surface mounted (NSM) technique. Validation study is conducted based on the experimental test available in the literature to investigate the accuracy of finite element models using LS-DYNA to present the behavior of the models. A parametric analysis is conducted on the effect of FRP bar diameters, number of grooves, groove intervals as well as width and height of the grooves on the flexural behavior of strengthened reinforced slabs. Performance of strengthening RC slabs with NSM FRP bars was confirmed by comparing the results of strengthening reinforced slabs with control slab. The numerical results of mid-span deflection and stress time histories were reported. According to the numerical analysis results, the model with three grooves, FRP bar diameter of 10 mm and grooves distances of 100 mm is the most ideal and desirable model in this research. The results demonstrated that strengthening of reinforced concrete slabs using FRP by NSM method will have a significant effect on the performance of the slabs.

Keywords: fiber reinforced polymer; finite element model; near surface mounted technique; RC slab

1. Introduction

A composite is defined as the assembly of two or more distinct materials to achieve new material whose overall performance is higher than the individual ingredients. FRP are composites that consist of two components: the fibres, which are the load carrying elements, and the matrix, which ensures the cohesion of the fibres, the retransmission of applied loads to the fibres, and the protection of fibres from the external environment (Shafigh *et al*. 2021). The matrix, such as a cured resin-like epoxy, polyester, vinyl ester, or other matrix acts as a binder and holds the fibres in the intended position, giving the composite material its structural integrity by providing shear transfer capability (Ibrahim *et al*. 2020). FRP products can take the form of bars, cables, two- and three dimensional grids, sheet materials, fabrics and laminates (Panahi *et al*. 2021). Two main methods in the implementation of FRP composites are the FRP EBR system and the NSM method, which is based on the placing strengthened materials in the grooves embedded in the surface (Fathuldeen and Qissab 2019). Among these new strengthening methods with use of CFRP, there is the NSM technique, which consists in the embedment of a CFRP strips or bars inside a groove performed in the strengthened element concrete, in order to optimize the exploitation of CFRP mechanical properties in favor of a more efficient RC structures strengthening.

Studies have shown that the assures higher shear and flexural strengthening effectiveness than the EBR technique (Al-zu'bi *et al*. 2022, Effiong and Ede 2022). Moreover, this NSM technique, in addition of decreasing the possibility of debonding failure, provides better resistance against fire (Al-Saadi *et al*. 2019). The NSM technique is based on the insertion of FRP reinforcement into the groove opened on the concrete tensile surface of RC structures to be strengthened (Zhang *et al*. 2021). As far as the structural performance of RC members is concerned, bond between FRP reinforcement and concrete is the most significant aspect that controls the structure's capacity, ductility, and serviceability. In this aspect, bond of GFRP and CFRP bars to concrete has been widely investigated, which resulted in a significant amount of experimental data on their bond performance (Noroozieh and Mansouri 2019). It was established that parameters such as concrete strength, bar diameter, embedment length, and concrete confinement significantly affect the bond performance of FRP bars to concrete. Bond development is strongly dependent on the mechanical and physical properties of the surface of the FRP bar and the constituents of the FRP material. It varies widely between different FRP bars due to the unique properties of each bar. In the following sections, the

*Corresponding author, Ph.D., Professor,
E-mail: zhangcw@sut.edu.cn
[a] Ph.D., E-mail: masoud.a877@yahoo.com

ISSN: 2287-5301 (Print), 2287-531X (Online)

parameters influencing the bond performance of FRP bars to concrete are highlighted.

Many research studies have reported that bond strength of FRP bars is inversely proportional to the bar diameter (Godat *et al*. 2021, Solyom and Balázs 2020, Thakur *et al*. 2021). Sayed (Ahmad *et al*. 2011) tested 60 pullout specimens to evaluate the effect of the bar diameter on the bond of CFRP bars to ultra-high-performance fiber-reinforced concrete. Four diameters (8, 10 and 12 mm for smooth bars and 7.5 mm for sand-coated bars) were used with embedment lengths of (5, 10, 15 and 20 d), "The authors concluded that specimens with shorter embedment length and smaller bar diameter developed the highest bond strength. Alvarez reported similar conclusions from testing 72 concrete cylinders (150 × 300 mm) reinforced with four different sand-coated GFRP bars (Alvarez-Villarreal 2004).

Numerical analysis of FRP strengthened beams has been correspondingly carried out for simulating the experimental results (Kocak 2015). Many researchers simulated the considering perfect bond conditions (no-slip occurrence) due to observing no debonding failure between CFRP-epoxy-concrete connections in the experimental tests (Almassri *et al*. 2016, Bui *et al*. 2022, Firmo *et al*. 2018). FE modeling of NSM CFRP strengthened beams considering debonding effects is, however, very limited (Hawileh 2012). Moreover, FE analysis of RC structures strengthened with prestressed NSM CFRP reinforcement is rarely carried out by taking into account the debonding effects (Omran and El-Hacha 2012). Besides, the numerical simulation of prestress procedure according to the adopted system in the experimental programs to prestress NSM FRP elements has never been considered in the FE analyses.

The aim of this study is to investigate flexural strengthening of reinforced concrete slabs with near surface mounted FRP bars. For this purpose, numerical investigations were conducted by finite element software LS-DYNA. The solutions were compared to those presented in literature, and the influence of effective factors including, FRP bar diameters, number of grooves, groove intervals as well as width and height of the groove on the load carrying capacity of reinforced concrete slabs sustained a concentrated load was then investigated.

2. Development of finite element model

Due to limitations in computing technology in the past, many structural analyses were conducted based on the SDOF model. Although the SDOF method is capable of providing engineers a reasonable estimation of structural response, it cannot provide detailed analysis on the localized structural failure under extreme blast loading. Nowadays, FE method is more commonly applied for structural analysis and in particular it has become a necessary tool to model and simulate reinforced concrete system. The reinforced concrete slab was modelled by using the LS-DYNA software. The program has a library which contains elements and constitutive models suitable for concrete and steel, and it was used for the modelling. In this research, a reinforced concrete slab with dimensions of 4 × 1 m with a thickness of 20 cm is considered. The five

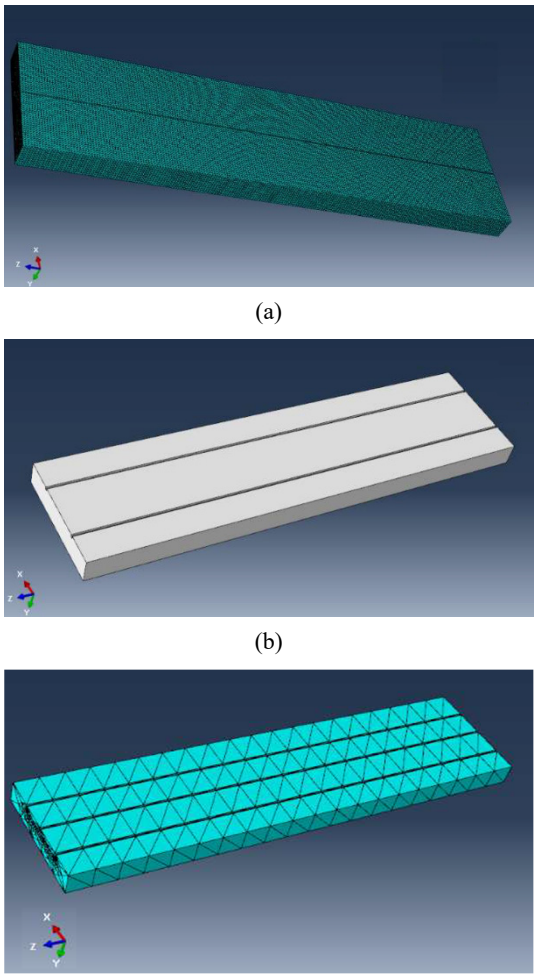

(a)

(b)

(c)

Fig. 1 Finite element modeling of RC slab strengthened with (a) one groove; (b) two grooves; and (c) three grooves

longitudinal tensile rebars with diameter of 8 mm and spacing of 15 cm is simulated in x direction and transverse rebars with diameter of 8 mm and spacing of 15 mm is considered in y direction. The cover of concrete is 5 cm in each direction. The slab was modelled as one-way slab fixed at the two opposite sides in the direction of bottom reinforcement. This model is selected as baseline model and other modeling samples with changes in the parameters studied in this research. Finite element modeling of RS slab strengthened with one groove, two grooves and three grooves are presented in Fig. 1. Table 1 gives the material properties of the concrete and steel reinforcement. The properties of the elements for steel reinforcement and concrete are defined using the keyword SECTION. In the simulation using explicit solver, all the loads, including gravity loads, are applied as dynamic loads.

2.1 Element formulation

Adequate mesh size and appropriate element type are important in performing finite element analysis, especially for dynamic blast analysis. The main reason is because they are the key factors that ensure all frequencies generated

Table 1 Material properties of concrete and steel reinforcement

Parameters	Rebar	Concrete
Density	7800 kg/m^3	2400 kg/m^3
Elastic Young's Modulus	200 GPa	30000 MPa
Longitudinal and transverse rebar yield stress	460/250 MPa	-
Poisson's ratio	0.3	0.2
Plastic strain at failure	12%	-
Uniaxial compressive/tensile strength	-	42/6.0 MPa

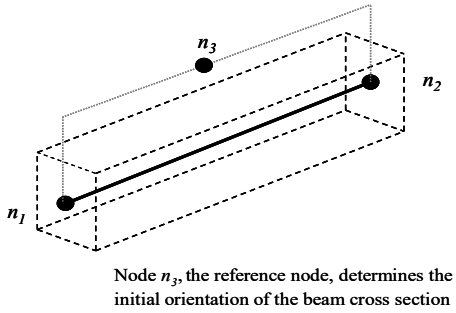

Fig. 2 LS-DYNA beam element (LS-DYNA 2007)

from blast waves are captured by each of the elements. In this research, appropriate mesh size is determined by halving the size of mesh in finite element models. It indicates the mesh size of 50 mm is suitable for analysis and further reduction in element size has insignificant effects on the results. Another reason to select the mesh size is computational cost. Therefore 50 mm mesh size is selected to reduce the computational cost.

The LS-DYNA 8-node hexahedron solid element is used to simulate concrete that it is defined by the keyword ELEMENT_SOLID. To define the element formulation and integration rule, the SECTION_SOLID keyword is used (Abedini and Zhang 2021b). The element formulation is determined by ELFORM variable option, and by default, ELFORM = 1 which denotes that the element is constant stress solid and uses one point (reduced) integration element. This option of formulation is known to be efficient, accurate and works on severe deformations. In addition, it requires less time in the analysis process. The use ELFORM = 2 option gives a fully integrated brick element formulation similar to the constant stress solid element. The disadvantage of ELFORM = 2 is that it requires more time in the analysis than ELFORM = 1. Also, in many situations it provides too stiff response and instability in large deformation applications. Therefore, ELFORM = 1 was used for the concrete solid elements formulation. However, this type of formulation requires the control of the zero energy modes which arise, called hourglassing modes. The 2-node Hughes-Liu beam element with 2 × 2 Gauss quadrature integration is employed for modelling all the 460 MPa yield strength steel reinforcements. It has several desirable qualities such as being simple and robust, yet results generated are compatible with the use of brick elements as its formulation is based on a degenerated brick element formulation. Each node of the created beam element has three rotational and three translational degrees of freedom. Initial orientation of the beam element can be achieved by specifying a reference node as shown in Fig. 2. The beam element takes into account the axial, bending and torsional deformations, and is defined in LS-DYNA by using the keyword ELEMENT_BEAM which requires the input of start point (N_1), end point (N_2), and nodal point (N_3) to define the orientation of the principal r-s plane of the beam.

2.2 Material modelling

It is important to incorporate realistic material models to achieve a credible simulation of reinforced concrete structure, with appropriate physical parameters, into the finite element system. For this research, concrete and steel are modelled with the material models available in the commercial software LS-DYNA. Generally, the constitutive models require input parameters to develop several material relations such as tangential stiffness and failure surface which are involved in the finite element analysis. These parameters include the basic concrete material properties such as the unconfined compression strength, the ultimate tensile strength, mass density in addition to other properties that vary from a model to another. The theoretical basis and features of these models are presented.

2.2.1 Concrete material model

Concrete is a composite material composed of a mixture of cement paste and aggregate, and provides fair characteristics in compression. The Material Model 72Rel3 in LSDYNA developed by Karagozian & Case consulting engineering firm, is chosen due to its capability of reproducing the concrete behaviour under various stress conditions covering a number of important factors that are pertinent to the dynamic behaviours of concrete (Abedini and Zhang 2021a). This concrete model can give good estimation of the structure behaviour compared with the test results with its automatic generation. The K&C concrete damage model with its automated generation ability is normally used for modelling large scale structures with macro scale element sizes under impulsive load. The failure of a RC structure under impulsive load is normally compression-dominated, because in such a structure the steel reinforcement would undertake most of the tensile forces even if damage occurs in concrete due to tension or shear.

In the last decade, many reinforced concrete models have been developed by researchers to determine the

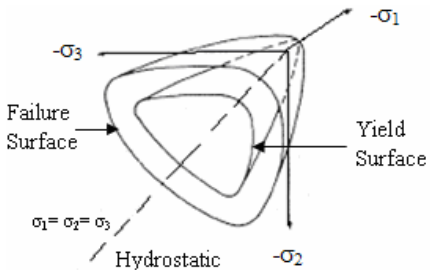

Fig. 3 Schematic failure surfaces of concrete material in three-dimensional stress space

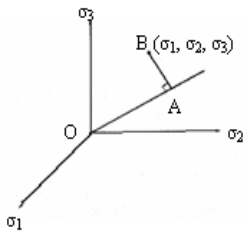

Fig. 4 Stress component in principal stress space

structural response when subjected to dynamic loading such as earthquake and blast loading (Abedini and Zhang 2021b, Zhang and Abedini 2022a, b). These concrete formulations can be categorized with regards to their damage function such as elasticity-based models, plasticity-based models, elasto-plastic damage models and plastic-fracturing models. Although these models have been proven to be highly satisfactory in estimating the structural response, further research in this field is still necessary in order to precisely define the complex behaviour of reinforced concrete.

It is necessary to consider both the uniaxial and triaxial stress states to construct the reinforced concrete material model accurately. To achieve this objective, precise failure criterion must be defined. Generally, concrete failure boundaries are defined as a region created by two surfaces namely the yield surface and the maximum failure surface in a three-dimensional principal-stress space as displayed in Fig. 3. From this figure, it can be seen that the maximum failure surface and yield surface are located in the principal stress space separated at some distance away from each other. Based on the findings from previous researchers, three failure modes can be identified when the concrete's loading surface intercepts the failure surface. The three failure modes are cracking, crushing and their combined effects.

For isotropic materials, like concrete, state of stress invariant functions is commonly used to develop the failure criterion and in this present study the concrete material failure criterion is defined by the stress invariants. With the stress tensor, σ_{ij}, the basic component of stress invariant functions is defined as the summation of two components namely deviatoric stress tensor, S_{ij} and hydrostatic stress tensor, $\sigma_h\delta_{ij}$. The general expression of σ_{ij} is as follows

$$\sigma_{ij} = s_{ij} + \sigma_h\delta_{ij} \tag{1}$$

and the pure hydrostatic stress is of the form

$$\sigma_h = \frac{1}{3}\left(\sigma_x + \sigma_y + \sigma_z\right) \tag{2}$$

Where σ_x, σ_y and σ_z are the principal stresses in x, y and z direction, respectively. By rearranging Eq. (2), the deviatoric stress, or the pure shear state equivalent, can then be calculated using the expression.

$$s_{ij} = \sigma_{ij} - \sigma_h\delta_{ij} \tag{3}$$

Both deviatoric and hydrostatic components are crucial to the concrete model as they govern the behaviour of the material. In this case, the hydrostatic component has a significant influence on the strain hardening of the concrete material and the deviatoric component determines the behaviour of concrete when compressive failure is experienced. For this concrete material the failure surfaces are constructed based upon the boundary created by the stress states (Zhang *et al*. 2020). The simplest representation of the stress state at a point in failure surface of a three-dimensional stress space is illustrated in Fig. 4.

From this figure, the vector OB represents the state of stress interested in which it can be divided into two components: OA, the hydrostatic component which lies along the hydrostatic axis, and AB, the deviatoric component which lies on a deviatoric plane and this plane is perpendicular to the hydrostatic axis. Both the hydrostatic and deviatoric planes can be constructed by the extension of their respective axis.

With the assistance of these defined planes, the shape of the concrete failure surface can then be easily described with the stress meridians. The stress meridians of the failure surface are characterized as the intersection curves of the failure surface and the meridian plane which is a plane consisting of hydrostatic axis. To successfully develop the shape of the failure surface, two extreme meridian planes are needed and they are known as the compressive and tensile meridian. These two meridian planes are characterized as the meridian planes that are farthest and closest intersections from the hydrostatic axis respectively. Using these planes, the triangular shape failure surface is simply defined by a point in the compressive meridian and a point in the tensile meridian. The path between the extreme meridians is defined by an elliptical curve as displayed in Fig. 5.

This two-dimensional failure plane can then be extended to represent the concrete material failure surface cross sections in a three-dimensional space. This is achieved by defining the interaction of curves between the failure

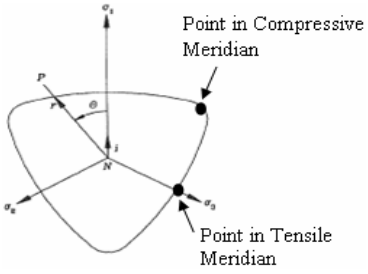

Fig. 5 Defining the deviatoric plane

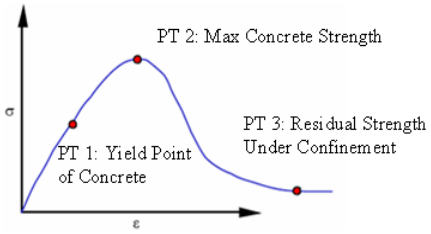

Fig. 6 Constitutive behaviour of concrete

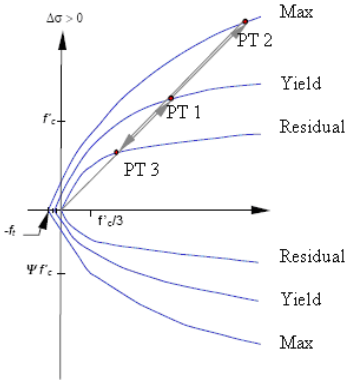

Fig. 7 Failure surfaces of concrete

surface and the deviatoric plane. Using the defined failure planes, the initial yield surfaces, strength envelope and subsequent stress-strain relationships can then be constructed to model the crushing and cracking behaviour of the concrete material under loading.

The constitutive behaviour of concrete under the impact loading is best described by the stress strain relation as shown in Fig. 6. During the initial loading stage, the deviatoric stress components maintain within the elastic region until the stress state reaches the initial yield surface which will onset the weakening of the material under the increasing load. Damage of the material will not be observed until the stress state increases to the maximum surface. Any increase in load beyond this stage will result in either permanent plastic response of the material or softening of material to a residual strength as shown in the Fig. 6.

Both concrete models employed in this study are developed with plasticity-based formulation with three pressure dependent failure surfaces as shown in Fig. 7.

The pressure on the failure surface of the concrete model is defined as

$$p = -\frac{1}{3}(\sigma_x + \sigma_y + \sigma_z) \tag{4}$$

where both pressure and stresses are positive in compression. Hence the curves in Fig. 7 that are above the p axis correspond to the compressive meridians and vice versa for the tensile meridians. As there is limited information regarding the material properties of the concrete, the self-generated concrete properties function offered by these two material models is used in the present study. In this case only the mass density and the unconfined concrete strength need to be specified into the computer

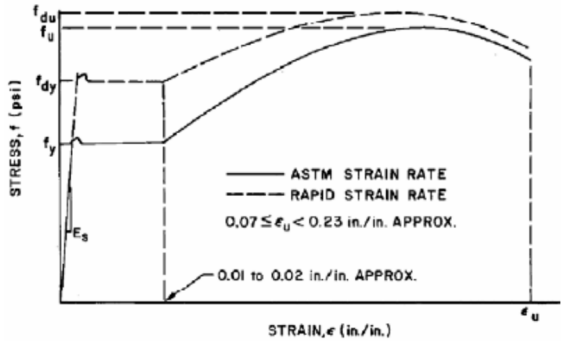

Fig. 8 Stress-strain curve for reinforcing steel

program. LS-DYNA will then generate various concrete properties based on the unconfined concrete strength of the concrete material. These properties include the tensile strength of the concrete (f'_t), the cohesion strength of concrete, pressure hardening coefficient for the failure surfaces and the scaled damage parameters under compression and tension stated previously.

2.2.2 Steel material properties

Steel is a critical component of reinforced concrete structures subjected to blast loads (Abedini and Zhang 2023). The inelastic response of metallic materials to dynamic loading can be easily monitored and assessed due to the isotropic properties. From past experimental data, it has been found that the yield strength can almost be doubled for mild steel under high strain rates; the ultimate tensile strength can increase by about 50% and the upper yield strength even higher. On the other hand, with increasing strain rate, the ultimate tensile strain decreases. Malvar provides a more detailed understanding of steel reinforcing bars under the effect of high strain rates. It has been observed that the failure strain for steel ranges between 13 to 20 percent. Hence, the failure criterion is based on the maximum principal strain criterion. Stress-strain curve for reinforcing steel can be seen in Fig. 8. In the current research material model Piecewise Linear Plasticity (material type 24) is used to simulate steel reinforcement in RC columns. Material Type 24 allows an arbitrary stress strain curve to be defined for an elasto-plastic material which was approximated to follow a bilinear stress strain curve in this research (Abedini and Zhang 2021a).

2.2.3 FRP material modelling

Material Type 58 (*MAT LAMINATED COMPOSITE FABRIC) in LS-DYNA was used to model the FRP material properties (Mutalib *et al*. 2013). Material Type 58 models composite materials with unidirectional layers, complete laminates and woven fabric. The properties of the FRP that were input into the material model are presented in Table 2. Epoxy adhesive is applied to externally bond the FRP to the column. The influence of the adhesive to the strength and rigidity of the composite is usually negligible. It protects individual fibers while providing a mechanism for load-transfer and shear resistance.

The Automatic_Surface_To_Surface_Tiebreak contact option in LS-DYNA was applied in this research to simulate the adhesive contact between the RC column and FRP. The

Table 2 Properties of FRP material (Chan *et al*. 2007)

Mechanical properties		Carbon/epoxy (AS4/3501-6)
Density (kg/m$^{3)}$	ρ	1580
Longitudinal modulus (GPa)	E_1	138
Transverse modulus (GPa)	E_2	9.65
In-plane shear modulus	G_{21}	5.24
Out-of-plane shear modulus	G_{23}	2.24
Minor Poisson's ratio	N_{23}	0.021
Through thickness Poisson' ratio	ν_{31}	0.021
Longitudinal tensile strength (MPa)	X_T	2280
Longitudinal compressive strength (MPa)	X_C	1440
Transverse tensile strength (MPa)	Y_T	57
Transverse compressive strength (MPa)	Y_C	228
In-plane shear strength (MPa)	S	71
Maximum strain for fibre tension (%)	ε_t	1.38
Maximum strain for fibre compression (%)	ε_c	1.175

Table 3 Epoxy adhesive properties by Syed-Ahmed

Property	**Value**
Tensile strength (*NFLS*)	32 MPa
Tensile modulus	11.7 GPa
Shear strength (*SFLS*)	29.4 MPa
Compressive strength	60 MPa
Poisson's ratio	0.2

adhesive properties of the FE models are defined according to Syed-Ahmed research work that presented in Table 3.

2.3 Contact option used in numerical simulations

The contact between longitudinal rebar and concrete is essential in the dynamic simulation since the stresses flow between materials affect the dynamic behavior of the structure (Abedini and Zhang 2022). In the current research, the interface between steel and concrete is modeled using the one-dimensional (1D) contact formulation. With this one-dimensional slide line contact type, steel nodes as slave nodes are dependent on concrete nodes as master nodes. When parts of common shared nodes are eroded from the simulation due to material failure, contacts between structural components need to be defined; otherwise, contacting parts that are not defined may intrude into the adjoining structural components without any counterforce. Interface bond in this contact type is defined as

$$\tau_{max} = G_s u_{max} e^{-h_{dmg} D} \quad (5)$$

Where τ_{max} is maximum shear stress in MPa, G_s is bond shear modulus in MPa, u_{max} is maximum elastic slip in mm, h_{dmg} is damage curve exponent and D is damage parameter.

2.4 Erosion of solid elements

After a solid element reaches a point where the strain is very large and pressure on it is low, it becomes insignificant in resisting load. When an element reaches this state, it should be deleted from the model as it does not provide resistance, and this can be done through erosion. The function MAT ADD EROSION in LS-DYNA is used to perform the function of deleting solid concrete elements when they no longer provide any resistance (Zhang and Abedini 2023). The failure criteria used for concrete in these models are the pressure at failure (Pmin) and the maximum principal strain at failure (εmax), "This means that an element will be eroded when the pressure in the element (P) is smaller than or equal to the pressure at failure (Pmin) or when the maximum principal strain (ε1) is larger than the principal strain at failure (εmax), "The tensile strength of concrete is known typically to be around 8 to 15 percent of its compressive strength. In this study the tensile compressive strength of concrete has been taken as 12.5 percent of the compressive strength. The principal failure strain taken for concrete varies through different types of studies. Some studies typically use 0.6, however in this study caution needs to be taken when considering the principal failure strain criterion for erosion. As the numerical model in the simplified analysis method is of larger element size than the pure blast simulation, a higher principal failure strain should be utilized. This is to stop large elements in the simplified numerical analysis being eroded or deleted to early, creating large voids in the structure. It can also be noted that deleting large portions of the model violates the conservation of mass. In order to make sure that the principal failure strain erosion criteria do not affect the results of the benchmark pure blast simulation, two pure blast simulations of erosion criteria of 0.6 and 0.9 principal failure strain are conducted.

2.5 Output files

The database definitions are used to obtain output files which contain results information. The output can be in the ASCII format by using the keyword DATABASE which contains many options. The options used, in addition to GLSTAT and MATSUM used for hourglass, BNDOUT is used to obtain the boundary condition forces and energy output file. Analysis results can be obtained graphically, and that includes geometry animations and time history plots for several characteristics (Zhang and Abedini 2021). This is done by importing binary output files to LS-PREPOST which are generated using the DATABASE_BINARY keyword.

3. Validation of numerical study

In order to validate the finite element models, the numerical study is validated against experimental research work done by Behzard *et al*. (2016). An experimental program was carried out to investigate the effectiveness of NSM method using CFRP bars for flexural strengthening of RC slabs with low clear cover thickness. Four full-scale RC

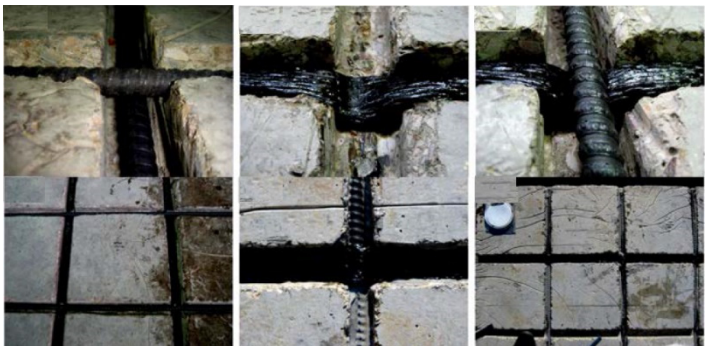

Fig. 9 Strengthening process of RC slab using NSM FRP rebar (Behzard *et al*. 2016)

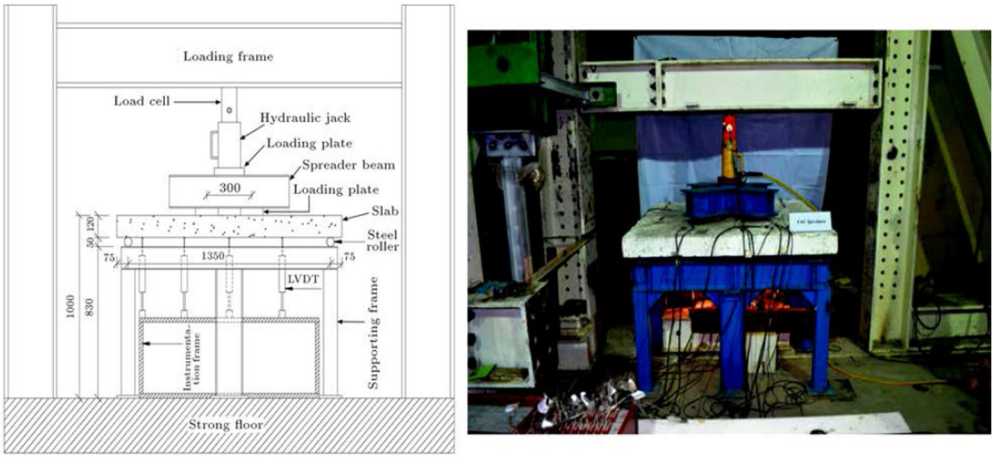

Fig. 10 Test setup and locations of the instruments (Behzard *et al*. 2016)

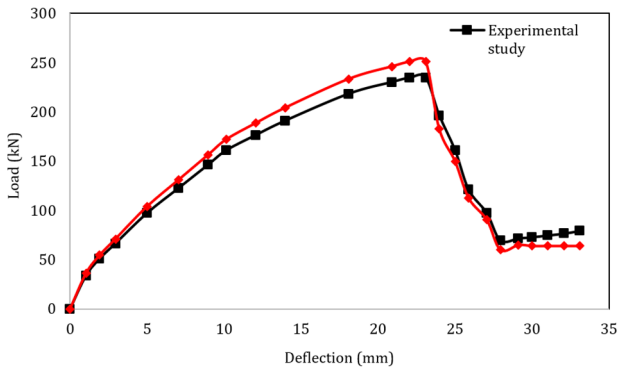

Fig. 11 Comparison of load deflection responses in experiment and numerical study

slabs (1500 × 1500 × 120 mm) were tested under monotonic four-point bending. One slab was kept un-strengthened as the control specimen and one slab was strengthened using NSM GFRP bars. Fig. 9 is presented the strengthening process of RC slab in (Behzard *et al*. 2016). Fig. 10 is presented test setup and locations of the instruments. Fig. 11 shows the load-central deflection responses of samples in the experimental test and the numerical analysis. The maximum load of the middle span is 234 kN and 250 kN in the experiment and the present numerical analysis, respectively thereby indicating a difference of only approximately 6%. The maximum load is found to be close to the experimental value. Therefore, we can conclude that by comparing the load-central deflection, the simulation results match the experimental observation.

4. Results and discussion

A parametric study is conducted to investigate the effect of different parameters including the FRP bar diameters, number of grooves, groove intervals as well as width and height of the groove on the flexural behavior of strengthened reinforced concrete slab with NSM FRP bars. Stress and deflections are important criteria in the analysis because structures are usually restricted to certain deflection values to attain specific reasonable damage levels. The deflection results for the RC slab were obtained from finite element analysis method using the LS-DYNA software.

4.1 Effect of FRP bars diameter

In this section, the influence of FRP diameter size is numerically investigated. The intended models consist of one groove in the bottom middle of RC slab strengthened with 10, 12 and 14 mm FRP bar. The stress and deflection time histories at mid-span of the RC slabs with and without strengthening systems are presented in Figs. 12 and 13, respectively. The stress of the strengthened beams increases with an increase in FRP bar diameter. In addition, the deflection of strengthened slabs increases with an increase

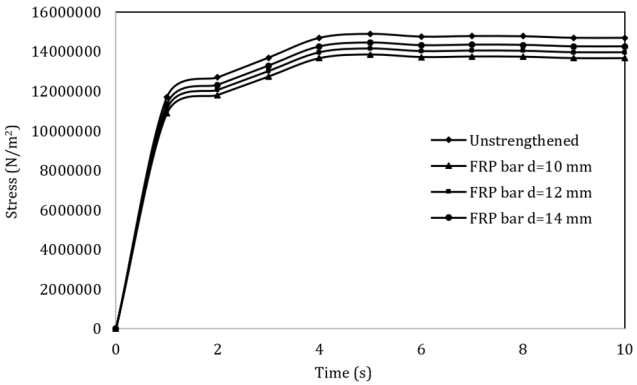

Fig. 12 Comparison of stress in RC slab strengthened with different FRP bar diameter

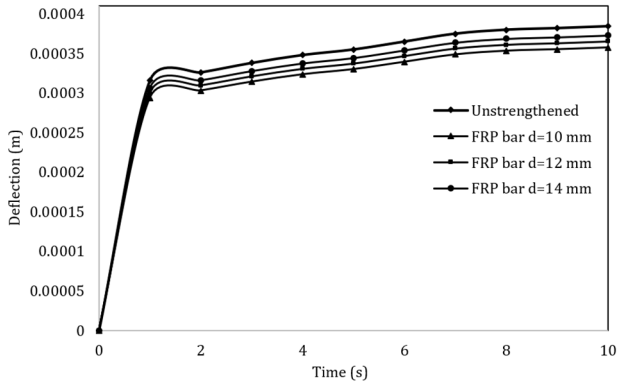

Fig. 13 Comparison of deflection in RC slab strengthened with different FRP bar diameter

in FRP bar diameter. The results demonstrated that the RC slab response increases by rising FRP bar diameters and the performance of the slabs will be more undesirable. It can be deduced by comparing the results of un-strengthened and FRP strengthened slabs that the RC slab response are less affected by different FRP bars diameter.

4.2 Effect of groove numbers

The effect of grooves numbers is investigated on models with constant values of FRP bar diameter and slab cross grooves numbers in load carrying capacity of RC slabs. section. Three different numerical models with groove numbers of 1, 2 and 3 are built to investigate the effect of Figs. 14 and 15 illustrate the results of stress and deflection time history with and without strengthening system. It is further observed that the maximum stress increases with decrease in the total groove numbers. Nevertheless, the deflection has decremental trend by increasing grooves numbers. Therefore, the ultimate load carrying capacity of the strengthened slabs increases with an increase in groove numbers. By increasing the number of grooves, the performance of the RC slabs will be more desirable. Also, the NSM FRP reinforcements reduced the strain in the internal steel bars and resulted in delay in the initiation and controlling propagation of the flexural cracks in slabs.

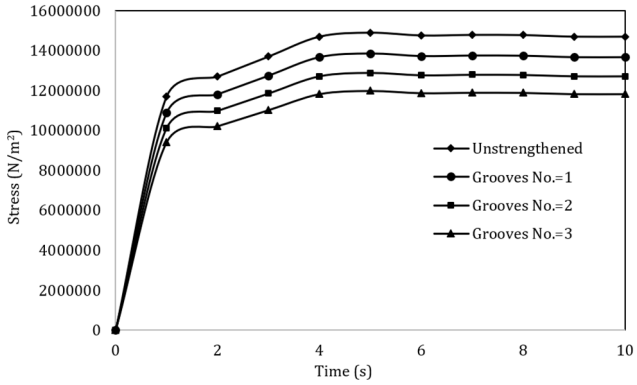

Fig. 14 Comparison of stress in RC slab strengthened with different groove numbers

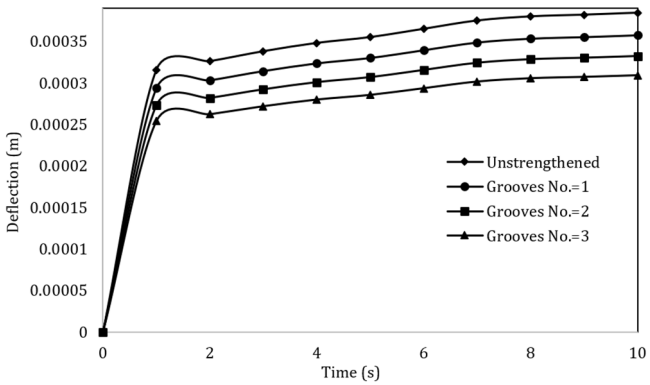

Fig. 15 Comparison of deflection in RC slab strengthened with different groove numbers

4.3 Effect of grooves intervals

Superimposed on Figs. 16 and 17 are the results of stress and deflection mid-span un-strengthened and strengthened RC slab by addressing the effect of groove intervals. The finite element models with cross-section dimension of 4 × 1 mm were used while the other effective factors were chosen as those mentioned before. In these models, three FRP bars with 10 mm diameter and three different groove distance namely 100, 150 and 200 mm were considered. It can be seen that the stress and ultimate deflection slightly vary with groove intervals. The stress of the strengthened slabs increases with an increase in grooves distance. In addition, the deflection of strengthened slabs increases with an increase in grooves distance. Therefore, the ultimate load carrying capacity of the strengthened slabs increases with decreases in groove distance. By increasing the groove distance, the performance of the RC slabs will be more undesirable.

4.4 Effect of width and height of the grooves

In this section influence of width and height of the grooves is numerically investigated. Three different numerical models with different width and height of the grooves namely 16, 18 and 20 mm were built and the

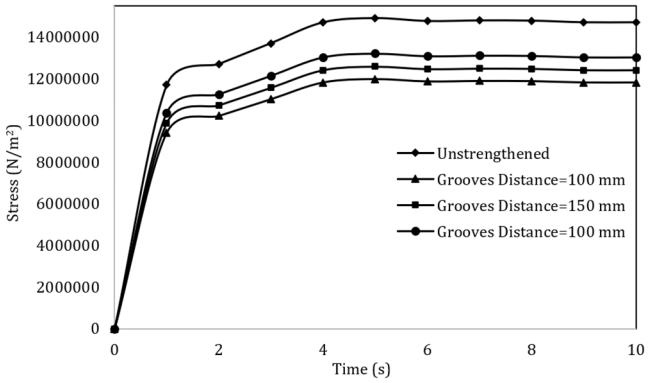

Fig. 16 Comparison of stress in RC slab strengthened with different grooves distance

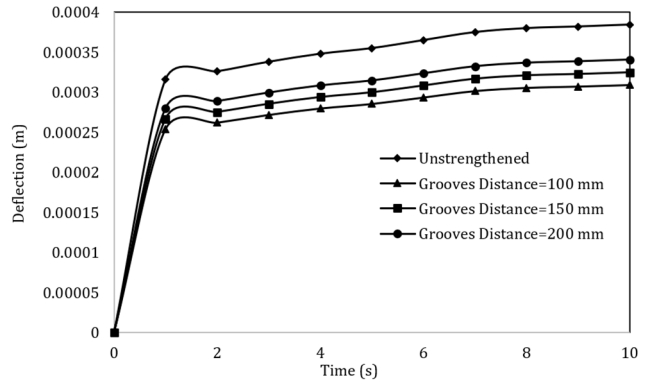

Fig. 17 Comparison of deflection in RC slab strengthened with different grooves distance

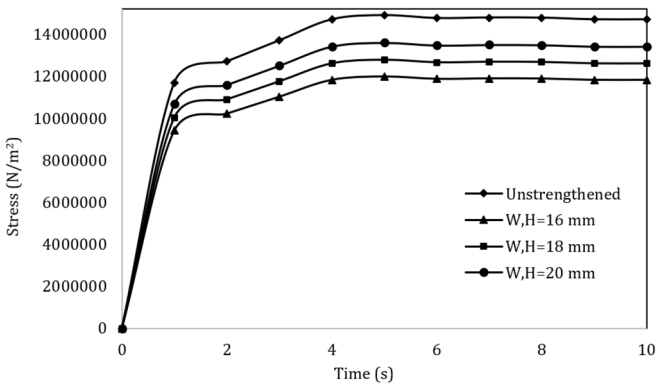

Fig. 18 Comparison of stress in RC slab strengthened with different groove width and height

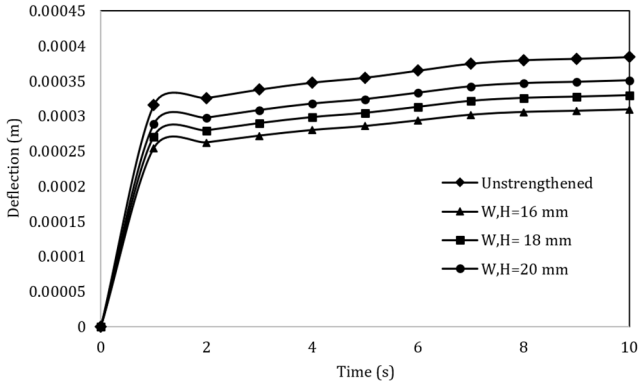

Fig. 19 Comparison of deflection in RC slab strengthened with different groove width and height

strengthened models compared to the control sample. The stress and deflection time histories at mid-span of RC slabs with and without strengthening systems are presented in Figs. 18 and 19, respectively. The stress of the strengthened slabs increases with an increase in width and height of the grooves. In addition, the deflection of strengthened slabs decreases with a reduce in width and height of the grooves. For the same configuration of strengthened slabs, the ultimate load carrying capacity of the strengthened slabs increases with decrease in width and height of the grooves. The results demonstrated that as the groove width and height increases, the RC slab response will decrease and the performance of the RC slabs will be more undesirable.

5. Conclusions

In the current study, strengthening of reinforced concrete slabs is performed by using near surface mounted (NSM) FRP technique. The analysis was performed using LS-DYNA non-linear FE code. The accuracy of the numerical models was verified using the findings of experimental data obtained by other researchers. The verified models were then used to simulate behavior of RC slabs strengthened with FRP bars. Parametric studies were conducted to investigate the effects of FRP bar diameters, number of grooves, groove intervals as well as width and height of the groove on flexural behavior of strengthened reinforced slabs. Based on the findings of the finite element analysis, the following conclusions can be drawn.

- The results demonstrated that the RC slab response increases by rising FRP bar diameters and the performance of the slabs will be more undesirable.
- The ultimate load carrying capacity of the strengthened slabs increases with an increase in groove numbers. Therefore, by increasing the number of grooves, the performance of the RC slabs will be more desirable.
- The stress of the strengthened slabs increases with an increase in grooves distance. In addition, the deflection of strengthened slabs increases with an increase in grooves distance.
- The ultimate load carrying capacity of the strengthened slabs increases with decrease in width and height of the grooves.
- The strengthened specimens had a stiffer behavior than that of the control specimen due to stiffening effect of FRP reinforcements.
- the NSM FRP reinforcements reduced the strain in the internal steel bars and resulted in delay in the initiation and controlling propagation of the flexural cracks in slabs.
- The results demonstrated that strengthening of reinforced concrete slabs using FRP by NSM method will have a significant effect on the performance of the RC slabs.

Acknowledgments

This research is financially supported by the National Natural Science Foundation of China (Grant No. 52361135807), the Ministry of Science and Technology of China (Grant No. 2019YFE0112400), and the Department of Science and Technology of Shandong Province (Grant No. 2021CXGC011204).

References

Abedini, M. and Zhang, C. (2021a), "Dynamic vulnerability assessment and damage prediction of RC columns subjected to severe impulsive loading", *Struct. Eng. Mech., Int. J.*, **77**(4), 441-461. https://doi.org/10.12989/sem.2021.77.4.441

Abedini, M. and Zhang, C. (2021b), "Performance assessment of concrete and steel material models in ls-dyna for enhanced numerical simulation, a state of the art review", *Arch. Computat. Methods Eng.*, **28**(4), 2921-2942.

Abedini, M. and Zhang, C. (2022), "Residual capacity assessment of post-damaged RC columns exposed to high strain rate loading", *Steel Compos. Struct., Int. J.*, **45**(3), 389-408. https://doi.org/10.12989/scs.2022.45.3.389

Abedini, M. and Zhang, C. (2023), "Dynamic performance of ultra-high performance fiber-reinforced concrete panel exposed to explosive loading", *Int. J. Protect. Struct.*, 20414196231212511. https://doi.org/10.1177/20414196231212511

Ahmad, F.S., Foret, G. and Le Roy, R. (2011), "Bond between carbon fibre-reinforced polymer (CFRP) bars and ultra high performance fibre reinforced concrete (UHPFRC): Experimental study", *Constr. Build. Mater.*, **25**, 479-485. https://doi.org/10.1016/j.conbuildmat.2010.02.006

Al-Saadi, N.T.K., Mohammed, A., Al-Mahaidi, R. and Sanjayan, J. (2019), "Performance of NSM FRP embedded in concrete under monotonic and fatigue loads: state-of-the-art review", *Austral. J. Struct. Eng.*, **20**(2), 89-114. https://doi.org/10.1080/13287982.2019.1605686

Al-zu'bi, H., Abdel-Jaber, M.T. and Katkhuda, H. (2022), "Flexural strengthening of reinforced concrete beams with variable compressive strength using near-surface mounted carbon-fiber-reinforced polymer strips [NSM-CFRP]", *Fibers*, **10**(10), 86. https://doi.org/10.3390/fib10100086

Almassri, B., Al Mahmoud, F. and Francois, R. (2016), "Behaviour of corroded reinforced concrete beams repaired with NSM CFRP rods, experimental and finite element study", *Compos. Part B: Eng.*, **92**, 477-488. https://doi.org/10.1016/j.compositesb.2015.01.022

Alvarez-Villarreal, A. (2004), "Temperature effect on bond properties of fiber Reinforced Polymer (FRP) bars embedded in concrete", Université de Sherbrooke.

Behzard, P., Sharbatdar, M.K. and Kheyroddin, A. (2016), "Different NSM FRP technique for strengthening of RC two-way slabs with low clear cover thickness", *Scientia Iranica. Transact. A, Civil Eng.*, **23**(2), 520. https://doi.org/10.24200/SCI.2016.2136

Bui, L.V.H., Jongvivatsakul, P., Stitmannaithum, B. and Likitlersuang, S. (2022), "Numerical modelling of bond mechanism of ETS FRP bar–concrete joints with long embedment length", *Int. J. Adhes. Adhes.*, **117**, 103179. https://doi.org/10.1016/j.ijadhadh.2022.103179

Chan, S., Fawaz, Z., Behdinan, K. and Amid, R. (2007), "Ballistic limit prediction using a numerical model with progressive damage capability", *Compos. Struct.*, **77**(4), 466-474. https://doi.org/10.1016/j.compstruct.2005.08.022

Effiong, J.U. and Ede, A.N. (2022), "Experimental investigation on the strengthening of reinforced concrete beams using externally bonded and near-surface mounted natural fibre reinforced polymer composites—a review", *Materials*, **15**(17), 5848. https://doi.org/10.3390/ma15175848

Fathuldeen, S.W. and Qissab, M.A. (2019), "Behavior of RC beams strengthened with NSM CFRP strips under flexural repeated loading", *Struct. Eng. Mech., Int. J.*, **70**(1), 67-80. https://doi.org/10.12989/sem.2019.70.1.067

Firmo, J., Arruda, M., Correia, J. and Rosa, I. (2018), "Three-dimensional finite element modelling of the fire behaviour of insulated RC beams strengthened with EBR and NSM CFRP strips", *Compos. Struct.*, **183**, 124-136. https://doi.org/10.1016/j.compstruct.2017.01.082

Godat, A., Aldaweela, S., Aljaberi, H., Al Tamimi, N. and Alghafri, E. (2021), "Bond strength of FRP bars in recycled-aggregate concrete", *Constr. Build. Mater.*, **267**, 120919. https://doi.org/10.1016/j.conbuildmat.2020.120919

Hawileh, R.A. (2012), "Nonlinear finite element modeling of RC beams strengthened with NSM FRP rods", *Constr. Build. Mater.*, **27**(1), 461-471. https://doi.org/10.1016/j.conbuildmat.2011.07.018

Ibrahim, M., Wakjira, T. and Ebead, U. (2020), "Shear strengthening of reinforced concrete deep beams using near-surface mounted hybrid carbon/glass fibre reinforced polymer strips", *Eng. Struct.*, **210**, 110412. https://doi.org/10.1016/j.engstruct.2020.110412

Kocak, A. (2015), "Earthquake performance of FRP retrofitting of short columns around band-type windows", *Struct. Eng. Mech., Int. J.*, **53**(1), 1-16. https://doi.org/10.12989/sem.2015.53.1.001

LS-DYNA (2007), "LS-DYNA Version 970 Keyword User's Manual", Livermore Software Technology Corporation.

Mutalib, A., Tawil, N., Baharom, S. and Abedini, M. (2013), "Failure probabilities of FRP strengthened RC column to blast loads", *Jurnal Teknologi*, **65**(2), 135-141.

Noroozieh, E. and Mansouri, A. (2019), "Lateral strength and ductility of reinforced concrete columns strengthened with NSM FRP rebars and FRP jacket", *Int. J. Adv. Struct. Eng.*, **11**(2), 195-209. https://doi.org/10.1007/s40091-019-0225-5

Omran, H.Y. and El-Hacha, R. (2012), "Nonlinear 3D finite element modeling of RC beams strengthened with prestressed NSM-CFRP strips", *Constr. Build. Mater.*, **31**, 74-85. https://doi.org/10.1016/j.conbuildmat.2011.12.054

Panahi, M., Zareei, S.A. and Izadi, A. (2021), "Flexural strengthening of reinforced concrete beams through externally bonded FRP sheets and near surface mounted FRP bars", *Case Stud. Constr. Mater.*, **15**, e00601. https://doi.org/10.1016/j.cscm.2021.e00601

Shafigh, A., Ahmadi, H.R. and Bayat, M. (2021), "Seismic investigation of cyclic pushover method for regular reinforced concrete bridge", *Struct. Eng. Mech., Int. J.*, **78**(1), 41-52. https://doi.org/10.12989/sem.2021.78.1.041

Solyom, S. and Balázs, G.L. (2020), "Bond of FRP bars with different surface characteristics", *Constr. Build. Mater.*, **264**, 119839. https://doi.org/10.1016/j.conbuildmat.2020.119839

Thakur, M.S., Pandhiani, S.M., Kashyap, V., Upadhya, A. and Sihag, P. (2021), "Predicting bond strength of FRP bars in concrete using soft computing techniques", *Arab. J. Sci. Eng.*, **46**(5), 4951-4969. https://doi.org/10.1007/s13369-020-05314-8

Zhang, C. and Abedini, M. (2021), "Time-history blast response and failure mechanism of RC columns using Lagrangian formulation", *Structures*, **34**, 3087-3098. https://doi.org/10.1016/j.istruc.2021.09.073

Zhang, C. and Abedini, M. (2022a), "Application of Lagrangian approach to generate PI diagrams for RC columns exposed to extreme dynamic loading", *Adv. Concrete Constr., Int. J.*, **14**(3), 153-167. https://doi.org/10.12989/acc.2022.14.3.153

Zhang, C. and Abedini, M. (2022b), "Development of PI model for FRP composite retrofitted RC columns subjected to high strain rate loads using LBE function", *Eng. Struct.*, **252**, 113580. https://doi.org/10.1016/j.engstruct.2021.113580

Zhang, C. and Abedini, M. (2023), "Strain rate influences on concrete and steel material behavior, state-of-the-art review", *Arch. Computat. Methods Eng.*, **30**(7), 4271-4298. https://doi.org/10.1007/s11831-023-09937-6

Zhang, C., Abedini, M. and Mehrmashhadi, J. (2020), "Development of pressure-impulse models and residual capacity assessment of RC columns using high fidelity Arbitrary Lagrangian-Eulerian simulation", *Eng. Struct.*, **224**, 111219. https://doi.org/10.1016/j.engstruct.2020.111219

Zhang, S., Ke, Y., Smith, S., Zhu, H. and Wang, Z. (2021), "Effect of FRP U-jackets on the behaviour of RC beams strengthened in flexure with NSM CFRP strips", *Compos. Struct.*, **256**, 113095. https://doi.org/10.1016/j.compstruct.2020.113095